Geophysical Journal International

Geophys. J. Int. (2013) **195,** 1464–1480
Advance Access publication 2013 October 3

doi: 10.1093/gji/ggt352

Occurrence conditions of roll waves for three grain–fluid models and comparison with results from experiments and field observation

M. Arai,[1] J. Huebl[2] and R. Kaitna[2]

[1] *Department of Civil Engineering, Faculty of Science and Technology, Meijo University, 468-8502 Nagoya, Japan*
[2] *University of Natural Resources and Life Sciences Vienna,* 1190 *Vienna, Austria. E-mail: roland.kaitna@boku.ac.at*

Accepted 2013 September 2. Received 2013 August 14; in original form 2013 January 23

SUMMARY

For the flow and deposition behaviour of debris flows, phenomena like particle sorting, levee formation and the development of roll waves are expected to be important processes. However, these processes are not well understood and hardly implemented in modelling approaches. In this study, we focus on the development of roll waves and derive advanced criteria separating stable and instable flow regimes for three debris flow models. These criteria are expressed using critical Froude numbers. Each of these simple flow models reflect different sources of flow resistance: laminar-viscous stress (Bingham type), dispersive stress due to particle collision (Bagnold type), and a model combining turbulent and dispersive stresses. Subsequently, we compare the predictions from these models with results from laboratory experiments with grain–fluid mixtures in a straight flume and with observations from a debris flow monitoring site at the Lattenbach creek in Austria. The experimental flows match with a turbulent flow model including particle collisions. For the natural flows the connection between models and observations is not clear due to limited field data. The results of our study contribute to an improved determination of critical flow conditions and provide data for model testing.

Key words: Instability analysis; Geomorphology; Geomechanics.

1 INTRODUCTION

Debris flows represent high concentrated mixtures of water and sediment of various type and sizes, from clay to boulders (DPRI 1994, 1999). Depending on the relative fraction of water, fine sediment (clay and silt) and coarse particles (gravel, pebbles and boulders), sources of energy dissipation may include: frictional and collisional resistance between the grains, viscous resistance of the fluid (which may carry fine and coarse particles in suspension), and interactions between the fluid and the solid phase like buoyancy, drag or fluid pressure in excess of hydrostatic (Iverson 1997; Armanini *et al.* 2005; Berzi & Jenkins 2008; Kaitna *et al.* 2011a). The relative importance of these processes is expected to depend on bulk composition (Takahashi 1980, 1991) and on scale (Iverson *et al.* 2010). However, even for steady-state flows systematic data on the relationship between material composition and relative importance of these processes are not yet available and only rough indications based on dimensionless numbers have been suggested (Savage and Hutter 1989, Iverson 1997; Ancey 2006). For natural debris flows processes like the development of a granular front (Suwa 1988; Kaitna *et al.* 2011b), levee formation (Johnson *et al.* 2012) or the development of surges (e.g. Arai *et al.* 2004, 2007; McCoy *et al.* 2010; Arai 2011, Fig. 1) add to the complexity of the phenomenon and may be of significant importance for flow propagation and deposition.

Debris flow triggering is mostly due to intensive rainfall events (see review by Guzzetti *et al.* 2008), however, a connection to earthquakes, volcanic activity or transformation from other processes have been described in literature (e.g. Haeberli *et al.* 2004; Evans *et al.* 2009; Liu *et al.* 2009). The mechanism of initiation may be sudden sediment supply to the channel system by bank failure or landsliding (e.g. Mikos *et al.* 2004), channel-bed failure due to hydraulic loading (e.g. Coe *et al.* 2008; Theule *et al.* 2012) or blockage and sudden release of material transported during a flood event. Based on hydraulic modelling and field observation Gregoretti and Fontana (2008) suggest a method to predict trigger conditions of debris flows due to run-off (channel-bed failure). The formation of surges during a debris flow event is possibly connected to these trigger mechanisms and availability of sediment for entrainment, however, detailed field data are rare. The formation of surges is often thought to result from progressive growth of roll waves when the channel length of a natural channel is sufficient. In large-scale flume experiments Iverson *et al.* (2010) observe the formation of roll waves which they attribute to the process of grain size segregation. Local patches of coarse sediment represent regions of higher resistance, inducing a progressive growth of wave fronts with gravelly snouts. Interestingly, amplitude and number of occurrence scales with an inverse power-law function, which may indicate a scale-free randomness of

Figure 1. Roll waves of a debris flow event in the Jang Jia Gully in China (Photo: Arai).

the described flow instabilities. The importance of longitudinal segregation effects on the formation and propagation of roll waves was also noted by Cristo *et al.* (2009).

Physical scale experiments on roll wave development were carried out with natural sediment–fluid mixtures and muddy slurries (e.g. Takahashi 1991; Coussot 1997), artificial grain–fluid mixtures (e.g. Davies 1988; Schonfeld 1996) and granular flows (e.g. Schonfeld 1996; Forterre & Pouliquen 2003). A general observation is that spontaneous roll wave formation without external forcing is connected to some flow intensity thresholds. Classical approaches explaining the formation of roll waves in debris flows are based on hydraulic theory (see review by Zanuttigh & Lamberti 2007). As there are flow conditions in a fluid where small perturbations can lead to a growth of the perturbation, debris flows are treated as single-phase, homogeneous fluids that travel over distances sufficiently long to develop roll waves. Studies focused on the formation and development of roll waves in laminar Newtonian flow (e.g. Benjamin 1957) and turbulent Newtonian flow (e.g. Jeffreys 1925). In his seminal work, Dressler (1949) provides a robust mathematical framework for describing roll wave formation in free surface flows of water (finite-amplitude wave theory). This approach was further developed for non-Newtonian, shear thinning fluids by Ng & Mei (1994), for shear-thickening fluids by Longo (2011) and for dry granular flows by Prasad *et al.* (2000). As pointed out by Longo (2011), most of the work done so far covers occurrence conditions for roll waves. Modelling of roll wave parameters like wave length, wave height or celerity is a more demanding task and not many approaches are yet available. A theoretical discussion of wave length is reported by Arai & Mizuyama (2011b).

The objective of this study is to discuss occurrence conditions of roll waves for different flow models and compare with experiments and field observations. Prediction of parameters like wave length and wave celerity needs an in-depth analysis of wave propagation in shallow water flows, which would go beyond the scope of this contribution and is therefore not discussed in this paper. Here, we derive new theoretical criteria for the occurrence of roll waves (Section 2) which are based on the theory of Dressler (Arai & Mizuyama 2011a) and connect them with three flow models that have been developed for describing the flow behaviour of concentrated grain–fluid mixtures like debris flows and debris floods (Section 3). The novelty of our approach is that the stability criterion includes a dependence on the shape of the flow cross-section, the friction factor and importantly the momentum correction factor for the velocity profile. We provide solutions for a turbulent shear stress model including particle collisions, a laminar flow model with a yield criteria (Bingham-type), and a dispersive stress model (Bagnold-type). Finally, we compare the predictions with results from laboratory experiments as well as field monitoring sites and discuss the possibility to draw conclusions on main sources of flow resistance for different types of flows (Section 4).

2 THEORETICAL OCCURRENCE CONDITIONS OF ROLL WAVES

2.1 Fundamental equations

The 1-D momentum and mass conservation equations for a homogeneous fluid flowing in an inclined channel read (Arai 2011)

$$\frac{\partial v}{\partial t} + \beta\, v \frac{\partial v}{\partial x} + (1-\beta)\frac{v}{A}\frac{\partial A}{\partial t} = g\sin\theta - g\cos\theta\frac{\partial h}{\partial x} - \frac{f'}{2}\frac{v^2}{R}, \tag{1}$$

and

$$\frac{\partial A}{\partial t} + \frac{\partial (A\, v)}{\partial x} = 0, \tag{2}$$

respectively. Here v is the cross-sectional mean velocity, A is the cross-sectional flow area, g represents acceleration due to gravity, θ is the slope angle of the channel, R is defined as the hydraulic radius, h is the depth of the flow, β represents a momentum correction factor, f' is a friction factor, x is the coordinate axis of flow direction and t is time. The first term on the left-hand side in eq. (1) represents acceleration of the flow, the second is a convective term and the third is a stress term due to depth fluctuations. On the right-hand side the first term represents the force due to gravity, the second is the force generated by surface slope inclination, and the third is friction loss.

For transforming momentum and mass conservation equations in a coordinate system moving with velocity c we define,

$$v(x,t) = U(x-ct) = U(\xi), \tag{3}$$

$$h(x,t) = H(x-ct) = H(\xi), \tag{4}$$

$$\text{here,} \quad \xi = x - ct. \tag{5}$$

U and H are functions of ξ, however it is possible for U to be expressed as a function of H and vice versa, therefore the partial differential operator is used as differentiation symbol to derive the mass and momentum equations in a moving reference framework

$$c\frac{\partial U}{\partial \xi} - \beta\, U\frac{\partial U}{\partial \xi} + c\,(1-\beta)\,\frac{U}{A}\frac{\partial A}{\partial H}\frac{\partial H}{\partial \xi} = -g\sin\theta + g\cos\theta\frac{\partial H}{\partial \xi} + \frac{f'}{2}\frac{U^2}{R}, \tag{6}$$

$$(U-c)\frac{\partial A}{\partial H}\frac{\partial H}{\partial \xi} + A\frac{\partial U}{\partial \xi} = 0. \tag{7}$$

Rearranged eqs (6) and (7) can be solved for flow depth and velocity gradients

$$\frac{\partial H}{\partial \xi} = \frac{-A\left\{g\sin\theta - \frac{f'}{2}\frac{U^2}{R}\right\}}{\{(\beta U - c)(U-c) + c(1-\beta)U\}\frac{\partial A}{\partial H} - g\,A\cos\theta}, \tag{8}$$

$$\frac{\partial U}{\partial \xi} = \frac{(U-c)\frac{\partial A}{\partial H}\left\{g\sin\theta - \frac{f'}{2}\frac{U^2}{R}\right\}}{\{(\beta U - c)(U-c) + c(1-\beta)U\}\frac{\partial A}{\partial H} - g\,A\cos\theta}. \tag{9}$$

Here, when $\partial H/\partial U$ is expressed as $\partial H/\partial U = (\partial H/\partial \xi)/(\partial U/\partial \xi)$ the right-hand side of eq. (8) can be substituted for $\partial H/\partial \xi$ and the right-hand side of eq. (9) for $\partial U/\partial \xi$ It then follows,

$$\frac{\partial H}{\partial U} = \frac{-A}{(U-c)\frac{\partial A}{\partial H}}.$$

Multiplying $\partial A/\partial H$ on both sides yields

$$\frac{\partial A}{\partial H}\cdot\frac{\partial H}{\partial U} = \frac{\partial A}{\partial U} = \frac{-A}{(U-c)}.$$

Using separation of variables, this expression is integrated

$$\int \frac{\mathrm{d}A}{A} = \int \frac{\mathrm{d}U}{c-U} + \ln K_A, \quad \text{here } \ln K_A \text{ is an integration constant,}$$

$$\ln A = -\ln(c-U) + \ln K_A,$$

$$\ln\{A\cdot(c-U)\} = \ln K_A,$$

and we obtain,

$$(c-U)\,A = K_A, \tag{10}$$

with $K_A =$ constant. We conclude that $(c-U)A$ is constant along the ξ-axis.

Substituting $U = c - K_A/A$ from eq. (10) to eq. (8), it can be written,

$$\frac{\partial H}{\partial \xi} = \frac{-A\left\{g\sin\theta - \frac{f'}{2}\frac{1}{R}\frac{(cA-K_A)^2}{A^2}\right\}}{\left\{\beta\left(\frac{K_A}{A}\right)^2 + (1-\beta)c^2\right\}\frac{\partial A}{\partial H} - gA\cos\theta} = -\frac{f_1(H)}{f_2(H)}, \tag{11}$$

where

$$f_1 = A\left\{g\sin\theta - \frac{f'}{2}\frac{1}{R}\frac{(c\,A-K_A)^2}{A^2}\right\}, \tag{12}$$

$$f_2 = \left\{\beta\left(\frac{K_A}{A}\right)^2 + (1-\beta)c^2\right\}\frac{\partial A}{\partial H} - g\,A\cos\theta. \tag{13}$$

2.2 Occurrence conditions for roll waves in an open channel flow

We use a linear flow instability condition suggested by Ishihara *et al.* (1954) and based on Dressler (1949) written as

$$\lim_{H\to H_0}\frac{\mathrm{d}H}{\mathrm{d}\xi}=\lim_{H\to H_0}-\frac{\mathrm{d}f_1/\mathrm{d}\xi}{\mathrm{d}f_2/\mathrm{d}\xi}\geq 0, \tag{14}$$

because it is valid for first step considerations.

A condition for a control cross-section can be defined with $f_1(H)=0$ and $f_2(H)=0$. $f_2(H)$ follows from eqs (13) and (10),

$$f_2(H)=\left(c^2-2\,\beta\,c\,U+\beta\,U^2\right)\frac{\partial A}{\partial H}-gA\cos\theta=0.$$

Here, from $R=A/S$, where S is wetted parameter and $F_r=U/\sqrt{gR\cos\theta}$ we obtain the expression $gA\cos\theta=gR\cdot S\cdot\cos\theta=U^2/{F_r}^2\cdot S$. If we substitute this into the above equation we obtain

$$c^2\frac{\partial A}{\partial H}-2\beta\,c\,U\frac{\partial A}{\partial H}+\left(\beta\frac{\partial A}{\partial H}-\frac{S}{{F_r}^2}\right)U^2=0.$$

When we multiply both sides of the above expression with $[\beta(\partial A/\partial H)-S/{F_r}^2]$ we obtain

$$\left\{\beta\frac{\partial A}{\partial H}c-\left(\beta\frac{\partial A}{\partial H}-\frac{S}{{F_r}^2}\right)U\right\}^2-\left\{\beta(\beta-1)\left(\frac{\partial A}{\partial H}\right)^2+\frac{S}{{F_r}^2}\frac{\partial A}{\partial H}\right\}c^2=0.$$

From eq. (10) we know that $K_A>0$, if $c>U$. In that case $U/c<1$. Since the cross-sectional area A increases with H, $\partial A/\partial H>0$ and the momentum correction factor β is $\beta\geq 1$. Of the two solutions

$$\frac{U}{c}=\frac{\beta\dfrac{\partial A}{\partial H}\pm\sqrt{\beta(\beta-1)\left(\dfrac{\partial A}{\partial H}\right)^2+\dfrac{S}{{F_r}^2}\left(\dfrac{\partial A}{\partial H}\right)}}{\beta\dfrac{\partial A}{\partial H}-\dfrac{S}{{F_r}^2}} \tag{15}$$

only that with the negative sign can satisfy the inequality $U/c<1$. We restrict considerations to this case. Here, we describe the case of a rectangular cross-section in which the area is a linear function of H. From eq. (13),

$$\frac{\partial f_2}{\partial A}=-2\beta{K_A}^2A^{-3}\frac{\partial A}{\partial H}+\beta{K_A}^2A^{-2}\frac{\partial}{\partial A}\left(\frac{\partial A}{\partial H}\right)+c^2(1-\beta)\frac{\partial}{\partial A}\left(\frac{\partial A}{\partial H}\right)-g\cos\theta$$

and with A as a linear function $\partial(\partial A/\partial H)/\partial A=0$, the expression

$$\frac{\partial f_2}{\partial A}=-2\beta{K_A}^2A^{-3}\frac{\partial A}{\partial H}-g\cos\theta \tag{16}$$

is obtained. In a rectangular cross-section of width B, the area A is calculated with $A=B\cdot H$ and consequently, $\partial A/\partial H>0$. Therefore, and using eq. (15), we conclude $(\partial\xi/\partial H)(\partial H/\partial A)>0$, and from eq. (16) we infer $\partial f_2/\partial A<0$. From $\partial f_2/\partial A=(\partial f_2/\partial\xi)(\partial\xi/\partial H)(\partial H/\partial A)$, the expression $\partial f_2/\partial\xi<0$ ensues. Consequently,

$$-\frac{\partial f_2}{\partial\xi}>0. \tag{17}$$

Moreover, we can conclude that $(\partial f_1/\partial\xi)/(\partial f_2/\partial\xi)$ in eq. (14) is

$$\frac{\partial f_1/\partial\xi}{\partial f_2/\partial\xi}=\frac{(\partial f_1/\partial A)(\partial A/\partial\xi)}{(\partial f_2/\partial A)(\partial A/\partial\xi)}$$

and from this and eqs (17) and (14) it follows,

$$\frac{\partial f_1}{\partial\xi}\geq 0 \tag{18}$$

and

$$\frac{\partial f_1}{\partial A}\geq 0. \tag{19}$$

Therefore,

$$\frac{\partial f_1}{\partial A}=g\sin\theta-2\,c\,\frac{f'}{2}\,(cA-K_A)\,A^{-2}\,S-\frac{f'}{2}\,(cA-K_A)^2\,A^{-2}\frac{\partial S}{\partial A}-\frac{1}{2}\,(c\,A-K_A)^2\,A^{-2}\,S\frac{\partial f'}{\partial A}+f'\,(c\,A-K_A)^2\,A^{-3}\,S\geq 0.$$

If for $UA\neq 0$, both sides of this expression are multiplied with $(1/g)\{1/(c\,A-K_A)^2\}A^3/(Sf')$ and the inequality

$$\frac{\sin\theta}{(cA-K_A)^2}\frac{A^3}{S\,f'}-\frac{c}{g}\frac{A}{(cA-K_A)}-\frac{1}{2\,g}\frac{A}{S}\frac{\partial S}{\partial A}-\frac{1}{2\,g}\frac{A}{f'}\frac{\partial f'}{\partial A}+\frac{1}{g}\geq 0 \tag{20}$$

is obtained. From the condition for the control cross-section $f_1 = Ag\sin\theta - (f'/2)(cA - K_A)^2 \cdot A^{-2} \cdot S = 0$, we derive

$$\sin\theta = \frac{f'}{2g}\frac{(cA - K_A)^2}{A^3}S, \tag{21}$$

and from eq. (10), we get

$$\frac{A}{(cA - K_A)} = \frac{1}{U}. \tag{22}$$

Substituting eqs (21) and (22) into eq. (20) yields

$$1 - 2\frac{c}{U} - R\frac{\partial S}{\partial A} - \frac{A}{f'}\frac{\partial f'}{\partial A} + 2 \geq 0.$$

Consequently, from $R = AS^{-1}$ we get $\partial R/\partial A = (1/S)(1 - R\,\partial S/\partial A)$, and with $\partial f'/\partial A = (\partial f'/\partial R)(\partial R/\partial A)$, the above inequality takes the form

$$\left(1 - R\frac{\partial S}{\partial A}\right) - 2\frac{c}{U} - \frac{R}{f'}\left(1 - R\frac{\partial S}{\partial A}\right)\frac{\partial f'}{\partial R} + 2 \geq 0.$$

With $m := 1 - R(\partial S/\partial A)$, and U as control cross-section, but now expressed as U_0, we obtain from the above imbalance

$$\frac{m}{2}\frac{U_0}{c}\left\{1 + \frac{2}{m} - \frac{R}{f'}\left(\frac{\partial f'}{\partial R}\right)_0\right\} \geq 1. \tag{23}$$

To derive a modified expression for U/c, we multiply denominator and numerator of the right-hand side of eq. (15) with $\beta(\partial A/\partial H) + \sqrt{\beta(\beta-1)(\partial A/\partial H)^2 + (S/{F_r}^2)(\partial A/\partial H)}$ and thus obtain

$$\frac{U}{c} = \frac{\left(\beta\frac{\partial A}{\partial H}\right)^2 - \left\{\beta(\beta-1)\left(\frac{\partial A}{\partial H}\right)^2 + \frac{S}{{F_r}^2}\left(\frac{\partial A}{\partial H}\right)\right\}}{\left(\beta\frac{\partial A}{\partial H} - \frac{S}{{F_r}^2}\right)\left\{\beta\frac{\partial A}{\partial H} + \sqrt{\beta(\beta-1)\left(\frac{\partial A}{\partial H}\right)^2 + \frac{S}{{F_r}^2}\left(\frac{\partial A}{\partial H}\right)}\right\}}$$

$$= \frac{\left\{\beta\left(\frac{\partial A}{\partial H}\right) - \frac{S}{{F_r}^2}\right\}\left(\frac{\partial A}{\partial H}\right)}{\left(\beta\frac{\partial A}{\partial H} - \frac{S}{{F_r}^2}\right)\left\{\beta\frac{\partial A}{\partial H} + \sqrt{\beta(\beta-1)\left(\frac{\partial A}{\partial H}\right)^2 + \frac{S}{{F_r}^2}\left(\frac{\partial A}{\partial H}\right)}\right\}} = \frac{\frac{\partial A}{\partial H}}{\beta\frac{\partial A}{\partial H} + \sqrt{\beta(\beta-1)\left(\frac{\partial A}{\partial H}\right)^2 + \frac{S}{{F_r}^2}\frac{\partial A}{\partial H}}}.$$

Now, with U_0/c as given above, inequality (23) takes the form

$$\frac{\frac{\partial A}{\partial H}\cdot\frac{m}{2}\left\{1 + \frac{2}{m} - \frac{R}{f'}\left(\frac{\partial f'}{\partial R}\right)_0\right\}}{\beta\frac{\partial A}{\partial H} + \sqrt{\beta(\beta-1)\left(\frac{\partial A}{\partial H}\right)^2 + \frac{\partial A}{\partial H}\cdot\frac{S}{{F_r}^2}}} \geq 1. \tag{24}$$

Moreover, defining $\Psi_0 := (m/2)\{1 + (2/m) - (R/f')(\partial f'/\partial R)_0\}$, this inequality can be transformed to yield an expression for a critical Froude number including the momentum correction factor β,

$$\frac{\frac{\partial A}{\partial H}\cdot\Psi_0}{\beta\frac{\partial A}{\partial H} + \sqrt{\beta(\beta-1)\left(\frac{\partial A}{\partial H}\right)^2 + \frac{\partial A}{\partial H}\cdot\frac{S}{{F_r}^2}}} \geq 1,$$

$$\frac{\partial A}{\partial H}\cdot\Psi_0 \geq \beta\frac{\partial A}{\partial H} + \sqrt{\beta(\beta-1)\left(\frac{\partial A}{\partial H}\right)^2 + \frac{\partial A}{\partial H}\cdot\frac{S}{{F_r}^2}},$$

$$\left\{\frac{\partial A}{\partial H}(\Psi_0 - \beta)\right\}^2 \geq \beta(\beta-1)\left(\frac{\partial A}{\partial H}\right)^2 + \frac{\partial A}{\partial H}\cdot\frac{S}{{F_r}^2},$$

$$\left(\frac{\partial A}{\partial H}\right)^2\{{\Psi_0}^2 - (2\Psi_0 - 1)\beta\} \geq \frac{\partial A}{\partial H}\frac{S}{{F_r}^2},$$

and finally,

$$F_r \geq \frac{\sqrt{\frac{\partial A}{\partial H} \cdot S}}{\left(\frac{\partial A}{\partial H}\right)\sqrt{\Psi_0{}^2 - (2\,\Psi_0 - 1)\,\beta}}. \tag{25}$$

Eq. (25) is a key equation in the current study, because it first time defines a general occurrence condition of roll waves depending on not only Froude number but also on the shape of the channel cross-section $\partial A/\partial H$, S, Ψ_0 (which is a function of the friction coefficient f') and the momentum correction factor β.

Again, the suffix 0 indicates the control section. Based on the assumption that the channel is rectangular and the width B of the channel is much wider than the depth ($B \gg H$), the cross-section area $A = B \cdot H$, wetted perimeter $S = B + 2H \approx B$ and the hydraulic radius $R = A/S \approx H$, Therefore $\partial S/\partial A = 0$, $m = 1 - R(\partial S/\partial A) = 1$ and $\partial A/\partial H = B$. Consequently, inequality (25) can be simplified to

$$F_r \geq \frac{1}{\sqrt{\Psi_1{}^2 - (2\,\Psi_1 - 1)\,\beta}} \tag{26}$$

with

$$\Psi_1 = \frac{1}{2}\left\{3 - \frac{H}{f'}\left(\frac{\partial f'}{\partial H}\right)\right\}. \tag{27}$$

We see that the occurrence of roll waves depends on a friction factor f' and a momentum correction factor β, which reflects the vertical velocity distribution within the flow. The velocity distribution can be described by an individual flow model.

3 OCCURRENCE CONDITION OF ROLL WAVES FOR DIFFERENT FLOW MODELS

As described earlier, various flow models for debris flows have been suggested. Here we focus on three models, which represent different dominant energy dissipation processes and connect them with the critical flow condition derived with eq. (25): a turbulent flow model including particle collisions, a laminar flow model with a yield criterion (Bingham-type) and a pure Bagnoldian dilatant flow model.

(i) Turbulent shear stress flow model with particle collisions:
In this model the flow resistance combines shear stress due to turbulent mixing (first term on the right-hand side of eq. 28) and shear stress due to particle collitions based on Bagnold's dispersion model (Bagnold 1954). It assumes a linear sum of individual effects in the flow (Arai & Takahashi 1983, 1986).

$$\tau = \rho_m\,\ell^2\left(\frac{\mathrm{d}u}{\mathrm{d}y}\right)^2 + a_i\,\sin\alpha\sigma\,(\lambda d)^2\left(\frac{\mathrm{d}u}{\mathrm{d}y}\right)^2. \tag{28}$$

The turbulent mixing length ℓ is based on von K*á*rm*á*n's model, that is, $\ell = \kappa\,y$, where κ is the von K*á*rm*á*n constant. In a case of uniform particle concentration and uniform flow in a rectangular channel, the velocity distribution u is (Arai & Takahashi 1986)

$$\frac{u}{U_*} = \frac{1}{\kappa}\left\{\sinh^{-1}\left(\frac{Y}{\phi}\right) - \sinh^{-1}\left(\frac{Y_0}{\phi}\right)\right\} \tag{29}$$

and the mean velocity v takes the form

$$\frac{v}{U_*} = \frac{1}{\kappa}\left\{\sinh^{-1}\left(\frac{1}{\phi}\right) - \sinh^{-1}\left(\frac{Y_0}{\phi}\right) - \sqrt{1+\phi^2} + \phi\right\}. \tag{30}$$

Here, $Y = y/h$; y is the distance from the bottom, whilst Y_0 is the bed condition of the channel,

$$Y_0 = \frac{y_0}{h}\begin{cases}\text{smooth bed condition: } y_0 = \dfrac{a\,\nu_0}{U_*},\ a = \dfrac{1}{9.025} \\ \text{rough bed condition: } y_0 = b\,k_s,\ b = \dfrac{1}{30},\ k_s\text{: roughness height}\end{cases} \tag{31}$$

Moreover, $\phi^2 = \lambda^2(a_i \sin\alpha/\kappa^2)(\sigma/\rho_m)(d/h)^2$, where $\lambda = \{(C_*/C)^{1/3} - 1\}^{-1}$ represents a linear concentration; ρ is the density of the fluid, σ the density of the particles, C the volume concentration of the solids in the flow, C_* the packing concentration of the solids, d the particle diameter, $\rho_m = \rho + (\sigma - \rho)C$ the apparent density of the fluid including suspended particles, $a_i \sin\alpha$ a Bagnold constant (0.022), ν_0 the kinematic viscosity of water, $U_* = \sqrt{gH\sin\theta}$ the shear velocity and H the flow depth.

Then, the occurrence condition of roll waves for this model obtained from (26) takes the form

$$F_r \geq \frac{1}{\sqrt{\left\{\Phi + \left(\frac{3}{2} - \beta\right)\right\}^2 - \beta\,(\beta - 1)}}, \tag{32}$$

with

$$\beta = \left[\left\{\sinh^{-1}\left(\frac{1}{\phi}\right)\right\}^2 - 2\left\{\sqrt{1+\phi^2} + \sinh^{-1}\left(\frac{Y_0}{\phi}\right)\right\}\cdot\sinh^{-1}\left(\frac{1}{\phi}\right) + 2\left\{\sqrt{1+\phi^2} - \phi\right\}\cdot\sinh^{-1}\left(\frac{Y_0}{\phi}\right) + \left\{\sinh^{-1}\left(\frac{Y_0}{\phi}\right)\right\}^2 + 2\right]$$
$$\times\left[\sinh^{-1}\left(\frac{1}{\phi}\right) - \sinh^{-1}\left(\frac{Y_0}{\phi}\right) - \sqrt{1+\phi^2} + \phi\right]^{-2}, \tag{33}$$

$$\Phi = \left[\sqrt{1+{\phi_0}^2\left(\frac{d}{H}\right)^2} - \phi_0\left(\frac{d}{H}\right)\right]\left[\sinh^{-1}\left\{\frac{1}{\phi_0}\left(\frac{H}{d}\right)\right\} - \sinh^{-1}\left\{\frac{1}{\phi_0}\left(\frac{y_0}{d}\right)\right\} - \sqrt{1+{\phi_0}^2\left(\frac{d}{H}\right)^2} + \phi_0\left(\frac{d}{H}\right)\right]^{-1}. \tag{34}$$

The step-by-step derivation of this expression is given in Appendix A.

(ii) Laminar flow model with yield criterion

The shear stress of the generalized Bingham flow model can be written as,

$$\tau = \tau_\eta + f\left(\mu, C, d, \frac{\mathrm{d}u}{\mathrm{d}y}, \ldots\right)\frac{\mathrm{d}u}{\mathrm{d}y}, \tag{35}$$

where τ_η is a parametrization of a yield criterion. Takahashi *et al.* (1998) applied Phillips' dispersional stress approach (Phillips *et al.* 1992) to a viscous flow in an open channel and determined the free parameters by experiments. The resulting equation takes the form

$$\tau = \tau_\eta + \frac{\mu}{\left(1 - \dfrac{C}{C_*}\right)^{1.82}(1+\epsilon C)}\frac{\mathrm{d}u}{\mathrm{d}y}, \tag{36}$$

which corresponds to (35) with constant $f(\mu, C, d, \mathrm{d}u/\mathrm{d}y, \ldots)$. For uniform sediment concentration and rectilinear flow, the velocity distribution u is obtained as follows (Arai & Mizuyama 2011a):

$$\frac{u}{U_*} = \frac{1}{2}\varphi_c R_*\left[\left(1 - \frac{{U_{*_\eta}}^2}{{U_*}^2}\right)^2 - \left\{\left(1 - \frac{{U_{*_\eta}}^2}{{U_*}^2}\right) - \left(\frac{y}{h}\right)\right\}^2\right]; \tag{37}$$

where $\varphi_c = (1 - C/C_*)^{1.82}\ (1+\epsilon C)$, $R_* = U_* h/\nu$, $\nu = \mu/\rho_m$, $\rho_m = \{\rho + (\sigma - \rho)C\}$, $\epsilon = \sigma/\rho - 1$, ${U_{*_\eta}}^2 = \tau_\eta/\rho_m$, ${U_*}^2 = g h \sin\theta$ and τ_η is the yield stress. Integrating over depth yields the mean velocity v normalized by the bed shear velocity,

$$\frac{v}{U_*} = \frac{1}{2}\varphi_c R_*\left\{\frac{2}{3}{a_\eta}^2 - \left(2 - \frac{{U_{*_\eta}}^2}{{U_*}^2}\right)a_\eta + 2\left(1 - \frac{{U_{*_\eta}}^2}{{U_*}^2}\right)\right\}a_\eta, \tag{38}$$

or as demonstrated in Appendix B

$$\frac{v}{U_*} = \frac{1}{6}\varphi_c R_*\left(3 - a_\eta\right){a_\eta}^2. \tag{39}$$

Consequently, the occurrence condition of roll waves in this flow model is obtained from the imbalance (26) as follows:

$$F_r \geq \frac{1}{\sqrt{(3-\beta)^2 - \beta\ (\beta - 1)}}, \tag{40}$$

$$\beta = \frac{3\left\{60{\varphi_B}^2 - 2a_\eta\,\varphi_B\,(3 + 2\varphi_B) + {a_\eta}^2(3 + 45\,\varphi_B)\right\}}{5\left\{2\,{a_\eta}^2 + 6\,\varphi_B - 3\,a_\eta\,(1+\varphi_B)\right\}^2} \quad \text{or} \quad \beta = \frac{3\,\left(15 - 7a_\eta\right)}{5\,\left(a_\eta - 3\right)^2}, \tag{41}$$

or

$$F_r \geq \frac{1}{\sqrt{\dfrac{36 - 33\,a_\eta + 9\,{a_\eta}^2}{\left(a_\eta - 3\right)^2}}}, \tag{42}$$

where $a_\eta = y_\eta/h$, $\tau_\eta = \rho_m g \sin\theta\,(h - y_\eta)$, $\varphi_B = (1 - {U_{*_\eta}}^2/{U_*}^2) = a_\eta$. The step-by-step derivation of this expression is given in Appendix B.

(iii) Dilatant flow model

Bagnold (1954) showed that in highly sheared grain–fluid mixtures the dispersive stress due to particle collisions can be determined by

$$\tau = a_i \sin\alpha\,\sigma\ (\lambda\, d)^2\left(\frac{\mathrm{d}u}{\mathrm{d}y}\right)^2. \tag{43}$$

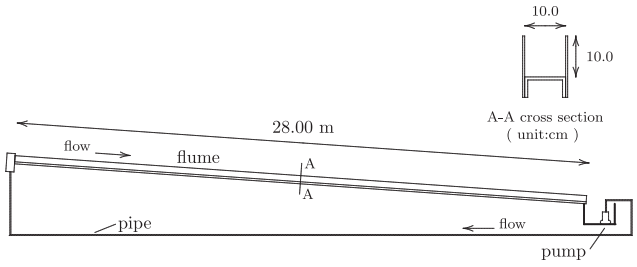

Figure 2. Side view and cross-section of the experimental flume.

Takahashi (1991) explained some characteristics of so-called stony type debris flows using Bagnold's theory and applied it to open channel flows. For uniform concentration and rectilinear flow, the velocity distribution u was obtained by Takahashi as follows:

$$\frac{u}{U_*} = \frac{2}{3}\left(\frac{h}{d}\right)\left[\frac{1}{a_i \sin\alpha}\left\{C + (1-C)\,\frac{\rho}{\sigma}\right\}\right]^{\frac{1}{2}}\left\{\left(\frac{C_*}{C}-1\right)^{\frac{1}{3}}-1\right\}\left\{1-\left(1-\frac{y}{h}\right)^{\frac{3}{2}}\right\}. \tag{44}$$

The mean velocity v can be calculated with

$$\frac{v}{U_*} = \frac{2}{5}\left[\frac{1}{a_i \sin\alpha}\left\{C + (1-C)\,\frac{\rho}{\sigma}\right\}\right]^{\frac{1}{2}}\left\{\left(\frac{C_*}{C}-1\right)^{\frac{1}{3}}-1\right\}\left(\frac{h}{d}\right), \tag{45}$$

with a constant momentum correction factor

$$\beta = \frac{5}{4}. \tag{46}$$

Therefore, the occurrence condition of roll waves follows in this flow model from (26) and is obtained as

$$F_r \geq \frac{2}{\sqrt{5}} \simeq 0.894. \tag{47}$$

The step-by-step derivation of this expression is given in Appendix C.

4 EXPERIMENTS AND FIELD OBSERVATIONS

4.1 Experiments

Experiments have been conducted in an experimental flume of 28 m length, 10 cm width and 10 cm depth (Fig. 2) erected at Meijo University, Japan. The cross-section is rectangular and the inclination of the flume can be adjusted between 0 and 5°. In a circulation system the tested solid–fluid mixtures are pumped from the exit of the flume back to the inlet, providing a constant discharge at the upstream end. The solid material used in the experiments consisted of non-cohesive coal particles with a d_{50} of 0.67 mm and a density σ of 1410 kg m^{-3}.

In this study the longitudinal gradient θ of the flume was varied between 0.5 and 3.0°. The discharge Q ranged between 1627 and 2945 cm^3 s^{-1}, creating flows with a mean flow depth h between 1.5 and 4.0 cm and mean velocity v between 63.5 and 156.8 cm s^{-1}. The ratio of mean flow depth to particle diameter h/d ranged from 22.4 to 59.7. The mean solid concentration by volume C ranged from 0.039 to 0.181. It seems that experimental solid concentrations are rather low compared to natural debris flows. However, in these small-scale experiments we do not aim to mimic prototype debris flows but want to investigate some basic effects associated with solid particles suspended in a fluid. Here we consider the fine particles as part of the fluid increasing its mean density and therefore the relative density of solids is decreasing in the flow.

Froude numbers F_r were calculated according to $F_r = v/\sqrt{gh\cos\theta}$ and the values varied between 1.17 and 4.09. We observe steady uniform flow for inclinations between 0.5 and 1°, with Froude numbers ranging from 1.18 to 1.41. For these experiments the sediment concentration ranged from 0.039 to 0.16. For flows at higher inclinations the onset of roll wave development was observed at Froude numbers between 1.59 and 4.09. Here sediment concentrations varied between 0.085 and 0.181.

4.2 Observations

Observations of roll waves in natural debris flows were made at an instrumented torrent in the Austrian Alps.

4.2.1 Study site

The watershed of the Lattenbach torrent has an area of 5.3 km^2 and is located in the western part of Austria. The Lattenbach torrent feeds the river Sanna, which is a tributary of the river Inn. The highest elevation in the watershed is around 2900 m above sea level (asl), the

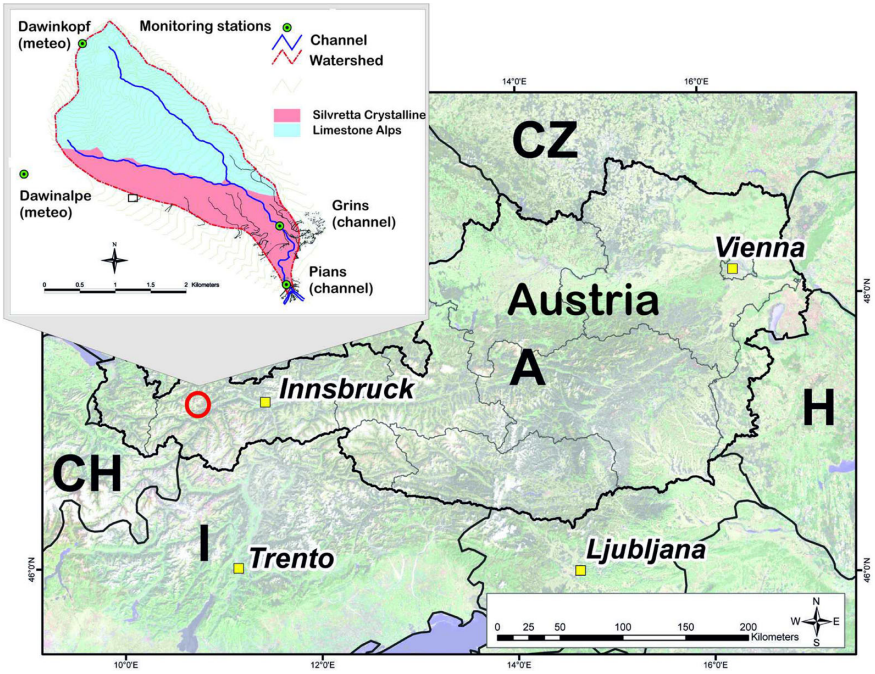

Figure 3. Location and geological setting of the Lattenbach creek, Austria, including an overview of the location of the monitoring stations (layers comprising administrative bodies and shaded relief provided by Environmental Systems Research Institute, Inc.).

confluence with the river Sanna at 840 mm asl. Both, the village Grins in the middle reach of the torrent and the village Pians at the outlet of the catchment, are affected by the hydrologic and geomorphic processes within the watershed. Geologically the catchment is located in the Northern Limestone Alps and Crystalline Alps in the southern part (Huebl *et al.* 2004). The tectonic transition between these geological units is marked by the left stem of the Lattenbach torrent (see Fig. 3). Due to intense mechanical loading of the rock and often unfavourable bedding of the strata parallel to the hillslope numerous mass wasting processes lead to a considerable debris potential for channel processes. Therefore, we assume that for debris flows and debris floods the availability of the transporting media is a limiting parameter rather than the availability of sediment. Severe events of debris flows and debris floods causing remarkable damage are reported in the years 1911, 1912, 1925, 1944, 1949, 1965, 1966, 1973 and 1998. The type and the intensity of the processes have been assessed based on the description of the damages and deposition volumes in the villages Grins and Pians (Huebl *et al.* 2004). Analysing the information for debris flow events in the chronicles, the most probable triggers result from rainfall events of short-duration and high intensity (thunderstorms).

4.2.2 Monitoring station

Since the year 2002 a monitoring station is operated by the Institute of Mountain Risk Engineering (University of Natural Resources and Life Sciences Vienna), recording meteorological data (rainfall, temperature, etc.) in the upper part of the catchment (station *Dawinalpe*) and run-off data from the middle and lower reach of the torrent at the villages *Grins* and *Pians*. Since the installation of this monitoring system two debris flow events were detected and recorded in the years 2007 and 2008.

The first channel monitoring station is located in a reach of a series of check dams close to the village *Grins*. This monitoring station comprises two ultrasonic based flow depth sensors (UPM-10, company Sommer, accuracy ± 10 mm) installed 5 m above two subsequent check dams 47 m apart. Due to the massive re-inforced concrete structures basal and lateral erosion is not to be expected (Fig. 4). The mean channel slope between the check dams is around 5 per cent and the average inclination of the channel reach is 13.3 per cent. The cross-section has an average basal width of around 7 m. The sampling interval initially was set to 10 min. The system was upgraded in 2007 to yield a sampling frequency of 1 Hz. The trigger condition for data recording is a threshold of a flow depth of 0.3 m measured at the upper sensor. Estimation of the roll wave velocity is based on cross-correlation of the two sensor signals. Using time-lag between corresponding sensor signals and knowing the distance between the sensors (47 m) yields the velocity.

The second monitoring station is installed about 130 m upstream of the confluence with the receiving river *Sanna* in a short bedrock reach within the municipality of *Pians*. The mean channel slope was determined as 3 per cent and the mean channel width varies between 2 and 4 m. The site is equipped with one ultra sonic flow depth sensor and two digital video cameras, one looking vertically down onto the flow surface and one recording the flow arriving from upstream (Fig. 5). The resolution is 720×576 pixels, with a frequency of 1 frame every 2 s. The video system is triggered together with the upper monitoring station *Grins*. To determine the spatial reference frame, the visible reach in both cameras was surveyed with a theodolite. Here, the roll wave velocity was estimated from video recordings of roll waves approaching the video camera monitoring a reach of around 80 m upstream. Corresponding peak flow depth from the ultrasonic sensor was used to calculate the Froude number. We estimate the accuracy of the flow stage from video analysis of less than 0.1 m and accuracy of peak velocity of 0.5 m s^{-1}.

Figure 4. Flow depth sensors installed over a series of check dams at the monitoring station Grins (middle reach).

Figure 5. Video and flow depth monitoring station Pians (lower reach).

Mean flow velocity between roll waves and flow depth was estimated from the bird-view camera recordings based on known reference points at the channel boundaries. Assuming a linear velocity distribution within the flow we estimated the mean flow velocity as half of the surface velocity derived with particle tracking. Due to the low frame rate this procedure was limited to low velocity flow conditions.

4.2.3 Observations

In late afternoon of 2007 June 20 a debris flow occurred in the course of a thunderstorm event. The meteo station *Dawinalpe* registered 55 mm of total rainfall within 130 min with a maximum intensity within 10 min of about 1.3 mm min^{-1}. Neighbouring regional weather stations did not register any precipitation. We anticipate the rainfall distribution over the catchment area to be highly variable, thus the measurements at our meteo station may not be representative for the whole catchment. We have limited information of the trigger mechanism for the subsequent debris flow. However, based on observations from field investigations in accessible reaches and aerial photographs we expect that the sediment was mainly mobilized from the northern stem (orographic left) of the channel by intensive hydraulic loading. This reach is affected by supply of colluvium of the limestone unit. However, landslides are distributed all over the upper regions of the watershed, feeding large volumes of fine sediment from the strongly weathered Crystalline unit (very soft phyllit) into the channel network (Huebl & Kaitna 2010). The debris flow event itself had a very high temporal variation, which could not be resolved by the sampling interval of 10 min at the monitoring station *Grins*. Therefore, we derive data from video analysis from the station *Pians*.

Based on the reconstructed hydrograph (Fig. 6) we derive an event volume of around 20 000 m^3. The event started at 5:02 p.m. and the last roll wave was observed at 5:28 p.m. In total 13 roll waves within 30 min were registered, each lasting not longer than 1 min. Velocities of the surges were measured between 5 and 10 m s^{-1}, with a peak value of 14 m s^{-1}. Between surges the velocity decreased considerably, coming nearly to a complete stop at a flow depth of around 1 m. The maximum discharge was around 200 m^3 s^{-1}. We estimated Froude numbers F_r using roll wave velocity and peak flow depth. Froude numbers between 0.83 and 2.29 were calculated. The debris flow event had a rather muddy appearance. Several big boulders (diameter around 1 m) could be identified only at the very front of the first roll wave (A1) from video recordings, but not in the deposits in the investigated lower reach of the Lattenbach creek. We expect that these large boulders were delivered to the receiving river *Sanna*. The event left the monitored reach between the flow depth sensors at Grins and the arch bridge without any considerable deposits within the channel, indicating high inertia and erosion potential of the material mixture travelling through this reach. Material samples were taken from deposits adjacent to the channel some weeks after the event using a shovel excavator. Subsequent grain size analysis showed that the material comprised a high fraction of fines (9 per cent silt and clay) and was mainly composed of sediment smaller

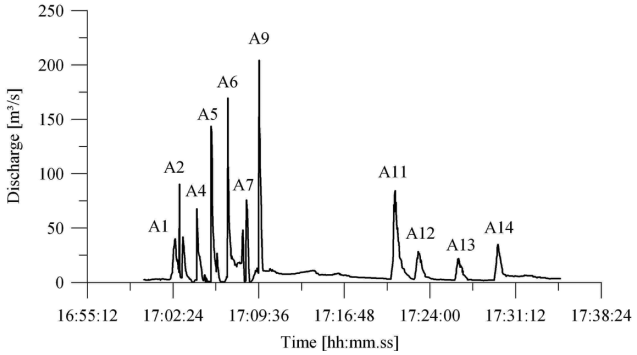

Figure 6. Hydrograph of the debris flow event 2007, derived from video analysis at the station Pians.

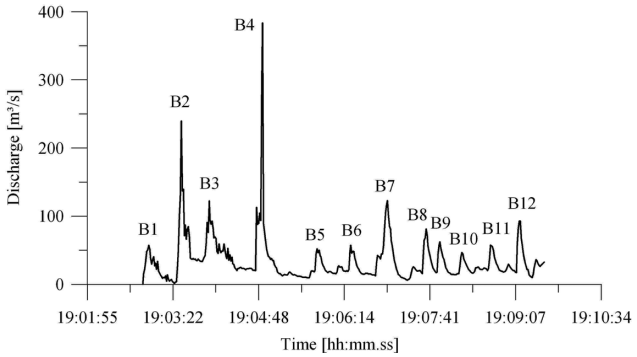

Figure 7. Hydrograph of the debris flow event 2008, derived from the paired flow depth sensors at the station Grins.

than 63 mm (82 per cent by weight). The maximum grain size of the sample material was 250 mm and the d_50 was determined with 8 mm. The complete grain size distribution curve is reported in Huebl & Kaitna (2010).

A smaller debris flow event occurred on 2008 September 1, between 7:01 p.m. and 7:10 p.m. For this event neither the data storage module of the climate station at *Dawinalpe* did work nor the video cameras at the lowermost station. However, data from neighbouring weather stations and reports from eye witnesses indicate the trigger to have been a local rainstorm event with high intensities during a short period of time. The hydrograph measured by the flow depth sensors at the station *Grins* is displayed in Fig. 7. During this event, 12 roll waves travelled with a mean velocity of around 6 m s^{-1} down the channel and delivered around 14 000 m^3 of material to the river *Sanna* within 6 min. Material composition and origin may be similar to the event in 2007, but no additional samples have been taken and no field investigation was carried out. The peak flow depth H_f varied between 1.0 and 4.1 m, with wave velocity V_f between 5.6 and 7.1 m s^{-1}. The peak discharge Q_f was estimated with 380 m^3 s^{-1} and Froude numbers F_r were between 1 and 2 (Table 2).

5 DISCUSSION

Limiting conditions to define the onset of roll wave development in Newtonian or non-Newtonian fluids are mostly expressed by a critical Froude number. The critical Froude number separating stable and instable turbulent flow of a Newtonian fluid is around 2. For laminar Newtonian flows the critical Froude number decreases to values between 0.5 and 0.6. Stability criteria for non-Newtonian rheologies, including power-law fluids (e.g. Ng & Mei 1994), viscoplastic fluids (e.g. Zanuttigh & Lamberti 2004) or dilatant fluids (e.g. Longo 2011) were derived by different authors (see the extensive review by Zanuttigh & Lamberti 2007). However, most of these approaches to determine critical conditions for roll wave development assume uniform flow velocities, that is, a momentum correction factor $\beta = 1$. Here we derive

Table 1. Summary of experimental parameters and results.

No.	θ (deg.)	Q (cm^3 s^{-1})	h (cm)	v (cm s^{-1})	C	h/d	F_r	Rem
1	3.0	1932	1.5	128.8	0.065	22.4	3.36	○ (roll wave)
2	3.0	2351	1.5	156.8	0.181	22.4	4.09	○
3	2.0	1654	1.8	91.9	0.085	26.9	2.19	○
4	2.0	1627	2.2	74.0	0.108	32.8	1.59	○
5	1.0	2889	3.5	82.5	0.134	52.2	1.41	• (non)
6	0.8	2398	3.2	74.9	0.091	47.8	1.34	•
7	0.8	1906	3.0	63.5	0.039	44.8	1.17	•
8	0.5	2945	4.0	73.6	0.160	59.7	1.18	•

Table 2. List of flow parameters derived for surges of the debris flow events at Lattenbach creek in 2007 and 2008.

No.	Surge no.	H_f (m)	V_f (m s^{-1})	Q_f (m^3 s^{-1})	F_r
1	A1	2.51	4.12	34.6	0.83
2	A2	3.48	6.55	90.4	1.12
3	A4	3.48	4.91	67.7	0.84
4	A5	4.14	8.17	143.5	1.28
5	A6	4.68	8.17	169.4	1.21
6	A9	3.67	13.75	204.3	2.29
7	A11	2.51	8.04	71.6	1.62
8	A12	1.14	6.80	28.4	2.03
9	A13	1.37	5.14	21.5	1.40
10	A14	1.32	8.10	32.5	2.25
11	B1	1.19	5.60	57.3	1.64
12	B2	2.96	7.10	239.7	1.32
13	B3	1.79	7.10	122.2	1.69
14	B4	4.10	7.14	383.7	1.13
15	B5	1.11	5.56	52.2	1.69
16	B6	1.19	5.60	57.3	1.64
17	B7	1.80	7.10	122.7	1.69
18	B8	1.44	6.30	81.3	1.67
19	B9	1.28	5.56	62.3	1.57
20	B10	1.01	5.56	47.7	1.77
21	B11	1.09	6.25	57.5	1.91
22	B12	1.64	6.25	92.8	1.56

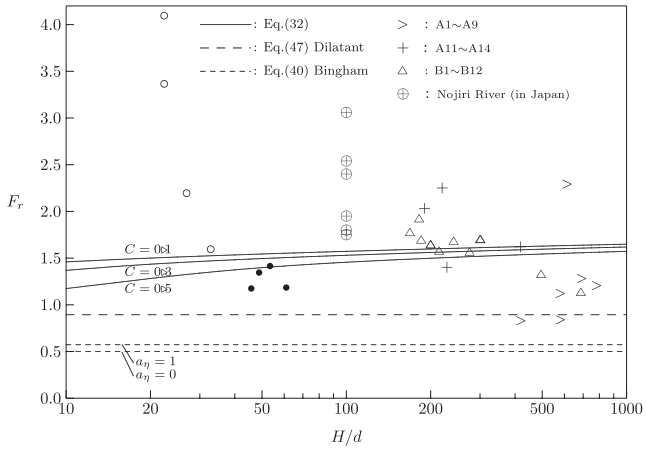

Figure 8. Relationship of Froude number F_r and length ratio H/d for identification of critical conditions for roll wave development. The symbols show experimental data (roll wave development is marked with '○', and stable flows with '●') and field observation, the lines represent predictions of the presented flow models.

equations for critical flow conditions depending on the shape of channel cross-section $\partial A/\partial H$, wetted parameter S, friction factor f' and the momentum correction factor β. Hence this approach can take into account variations of the velocity profile, reflecting different flow models, as well as different values of the respective friction parameters.

To compare experimental flow conditions and flow parameters estimated from field monitoring with thresholds derived for different flow models, Froude numbers F_r are plotted against relative flow depth H/d (Fig. 8). For the natural debris flows we use Froude numbers estimated as described earlier and the d_{50} determined from grain size analysis. The flow model combining turbulence and particle collisions (eq. 32) is plotted for varying depth ratios and volume concentrations of $C = 0.1$, 0.3 and 0.5 (solid lines). We see that the ratio of flow depth as well as grain concentration influence the occurrence of roll waves: when the concentration C is low, the critical Froude number F_r is higher than for high concentration flows. In other words, flows of low sediment concentration are more stable than flows of high concentration and for a constant Froude number the flow becomes instable when grain size increases. Comparing this model with experimental observations we see that the Froude number threshold between stable and instable flow fits very well with the theoretical results for sediment concentrations between 0.1 and 0.3, representing the range of the experiments. On the contrary, the Bagnoldian flow model (eq. 47, dashed line in Fig. 8), where particle collisions are pre-dominant, is insufficient to predict the onset of roll wave development. We suspect that in our experimental flows turbulence is significant and that the mixing length (scale of turbulent eddies) of the mixture of fluid and suspended sediment is large. The Bingham model can be interpreted as a laminar flow model with a yield criterion. $a_\eta = 1$ represents a situation when the material is

Figure 9. Screenshots from the video recording of the debris flow event at Lattenbach creek in 2007: (a) surge A1 including large boulders, (b) surge A4 having a highly viscous appearance and (c) turbulent surge A11.

sheared over the complete flow depth (i.e. no yield stress and no plug flow), and in case of $a_\eta = 0$ shear is concentrated in a narrow layer close to the bed (eq. 40, dotted lines in Fig. 8). It is interesting to see, that the existence of a yield criterion does not have a significant influence on the magnitude of the threshold Froude number separating stable and instable flow. Comparing this model with the experiments we see that the critical Froude number range predicted by the model is around 0.5–0.6, whereas the onset of roll waves in the experiments was observed at the Froude number of around 1.5. We therefore conclude that laminar flow resistance may not be a dominant process in our laboratory flows. Based on the available data from the monitoring stations we try to compare the model predictions with surges observed in the field. It is noted that our calculation of the theoretical occurrence condition of roll waves assumes uniform flow in a wide, rectangular channel. This simplification does not strictly agree with the actual conditions. We expect similar flows in a wider channel to have higher Froude numbers than calculated here, because the depth H_f is evaluated larger than the depth for the assumed conditions. For surges A11–A14 (+) of the event in 2007 and B1–B12 (△) of the event 2008 the threshold lines of the turbulent flow model including particle collisions match the observed Froude number range. However, surges A1–A9 (>) do not follow this trend. Video analyses reveal that the first surge in 2007 contained large boulders followed by a high concentrated mixture of high viscous consistency (Fig. 9a). For the roll waves A2–A9 the consistency of the flow was similar, however, no boulders could be detected (Fig. 9b). This is an important observation, because it confirms that debris flow surges are not necessarily connected to the presence of a granular front. Between these first surges flow velocity decreased dramatically although surface elevation remained high. Consequently also discharge was close to zero in the period from A1 to A9 (see Fig. 6). For this period (from surge A1 to A9 in Fig. 6) this fine grained, highly concentrated flow may be governed by laminar flow resistance, which is reflected by low Froude numbers fitting to the stability criterion of a laminar flow model. Video recordings show that in the course of the event the water content obviously increased and splashing of a more liquid fluid where visible for surges A11–A14 (e.g. surge A11, Fig. 9c). These surges, together with the surges of the event in 2008 had higher Froude numbers which direct to the higher threshold values of a turbulent-dispersive model. However, we do not have a comparing data set of stable flows with this flow composition, so we cannot rule out the validity of a laminar model. The same is true for surges observed at Frounde numbers above 1.5 in the Nojiri River in Japan. Here sediment particle size and flow surges were significantly smaller than the flow depth, pointing to a flow with turbulent mixing of sediment and fluid, which would be in agreement with the turbulent model including particle collisions. But again, due to the lack of more data, we cannot rule out other models.

The approach explaining roll wave formation in debris flows presented herein as well as in other studies (e.g. Zanuttigh & Lamberti 2002, 2007; Longo 2011) is based on hydraulic theory and represent strong simplifications of a prototype flow. Here, debris flows are regarded as homogeneous, incompressible fluids. Density variations and grain size segregation (longitudinal and vertical) are neglected. As shown by Iverson *et al.* (2010) variations of sediment concentration can cause local increased flow resistance and by that may govern growth and progression of flow perturbations. Roll waves observed in the Lattenbach creek may be influenced by these effects, although accumulation of large boulders was only visible at the first surge. We further cannot exclude the possibility that sudden input of sediment in the upper catchment and along the transport zone by landslides, bank failure and/or bed erosion is linked to the formation of the observed roll waves. The physical scale experiments presented in this study represent the grain–fluid mixtures of low solid concentration (<0.2) and are not intended to mimick the flow behaviour of prototype debris flows. However, the flow is expected to deviate from Newtonian flow and is expected to be a solid test for the instability criteria derived for the different flow models.

6 CONCLUSIONS

It is known that occurrence condition of roll wave is function of Froude number. In this contribution we present new threshold criteria for the occurrence of roll waves in concentrated sediment–fluid mixtures. We first derive a mathematical formulation that depends on not only Froude number, but also the shape of channel cross-section $\partial A/\partial H$, wetted parameter S, friction factor f', and the momentum correction factor β. Subsequently we apply this equation to three different debris flow models and derive stability criteria based on a critical Froude number. These simple one-phase models are not expected to fully represent internal flow mechanics of natural debris flows or debris floods. However, using simple approaches allows to derive criteria for separating stable and instable flows. Moreover, using such approaches may help to identify dominant sources for flow resistance. In this study we focused on turbulence, viscous friction in a laminar regime and dispersive pressure due

to particle collisions. The derived threshold values where compared with exact measurements from appropriate laboratory experiments and estimations from field observations at Lattenbach creek in Austria, which were based on flow depth measurements, video recording and grain size analysis after the field events. They indicate that these flows had a high fraction of fine sediment and therefore may be termed mudflows. In the case of quite liquid experimental surges (high water content) turbulent mixing of sediment and fluid is expected to be present. The occurrence of roll waves here is in accordance with the theoretical predictions from a turbulent flow model including particle collisions. For the observed natural surges of low water content and very viscous appearance Froude numbers are low, which point to the low threshold values of a laminar flow model. Due to limited field data, the match with other models or the influence of other processes like erosion or particle sorting for roll wave development cannot be ruled out. Notably the flow regime transforms within one event and roll waves develop also at higher Froude numbers at a later stage.

ACKNOWLEDGEMENTS

We thank Fritz Zott for technical support of the monitoring station. We also want to thank Matt Pike, Andreas Mursch-Radlgruber, Michaela Ferbar for supporting field work and data analysis. Dr. K. Hutter and an anonymous reviewer are particularly thanked for critical reviews that significantly improved of the manuscript.

REFERENCES

Ancey, C., 2006. Plasticity and geophysical flows: a review, *J. Non-Newtonian Fluid Mech.,* **142,** 4–35.

Arai, M., 2011. A fundamental study on occurrence mechanism of roll wave of debris flow and it's wave length and period, *Doctoral thesis,* Kyoto University Japan, pp. 10–12, in Japanese.

Arai, M. & Mizuyama, T., 2011a. Surge occurrence condition and flow models of muddy debris flow, *J. Jpn. Soc. Civil Eng., Ser. B1 (Hydraulic Engineering),* **67**(3), 92–100, in Japanese.

Arai, M. & Mizuyama, T., 2011b. A theoretical discussion of wave length on intermitent muddy debris flow surges, *J. Jpn. Soc. Civil Eng., Ser. A2 (Appl. Mech. (AM)),* **67**(2), I345–I354, in Japanese.

Arai, M. & Takahashi, T., 1983. A method for measuring velocity profiles in mud flows, in *Proceedings 20th International Congress,* International Association for Hydraulic Research, Vol. 3C, pp. 279–286.

Arai, M. & Takahashi, T., 1986. Mechnism of muddy debris flow, *J. Hydraulic, Coastal and Environ. Eng.,* **375**(II-6), 67–77, in Japanese.

Arai, M., Liu, X. & Tahara, N., 2004. A condition of occurrence on the roll wave of viscous debris flow, *J. appl. Mech.,* **7,** 813–820, in Japanese.

Arai, M., Horie, W. & Akie, M., 2007. Occurrence condition of the roll wave surges on the viscous debris flow regarded the flow mechanism, *J. appl. Mech.,* **10, 523**–532, in Japanese.

Armanini, A., Capart, H., Fraccorollo, L. & Larcher, M., 2005. Rheological stratification in experimental free-surface flows of granular-liquid mixtures, *J. Fluid Mech.,* **532**, 269–319.

Bagnold, R.A., 1954. Experiments on a gravity-free dispersion of large solid spheres in a Newtonian fluid under shear, *Proc. R. Soc. Lond.,* **225,** 49–63.

Benjamin, T.B., 1957. Wave formation in laminar flow down an inclined plane, *J. Fluid Mech.,* **2,** 554–574.

Berzi, D. & Jenkins, J.T., 2008. A theoretical analysis of free-surface flows of saturated granular-liquid mixtures, *J. Fluid Mech.,* **608,** 393–410.

Coe, J.A., Kinner, D.A. & Godt, J.W., 2008. Initiation conditions for debris flows generated by runoff at Chalk Cliffs, central Colorado, *Geomorphology,* **96,** 270–297.

Coussot, P., 1997. *Mudflow Rheology and Dynamics,* Balkema, 255 pp.

Cristo, C.D., Iervolino, M., Vacca, A. & Zanuttigh, B., 2009. Roll-waves prediction in dense granular flow, *J. Hydrol.,* **377,** 50–58.

Disaster Prevention Research Institute Kyoto University and Institute of Mountain Hazards and Environment Chinese Academy of Sciences and Ministry of Water Conservancy, 1994. Japan-China Joint Research on the Prevention from Debris Flow Hazards, 195 pp.

Disaster Prevention Research Institute Kyoto University and Institute of Mountain Hazards and Environment Chinese Academy of Sciences and Ministry of Water Conservancy, 1999. Japan-China Joint Research on the Mechanism and the Countermeasures for the Viscous Debris Flow, 206 pp.

Davies, T.R.H., 1988. Debris flow surges—a laboratory investigation, *Mitteilungen 96,* 122 pp., Versuchsanst. fur Wasserbau, Hydrol. und Glaziol. an der ETH Zuerich, Zuerich, Switzerland.

Dressler, R.F., 1949. Mathematical solution of the problem of roll-waves in inclined open channels, *Commun. Pure Appl. Math.,* **2**(2/3), 149–194.

Evans, S.G., Bishop, N.F., Smoll, L.F., Murillo, P.V., Delaney, K.B. & Oliver-Smith, A., 2009. A re-examination of the mechanism and human impact of catastrophic mass flows originating on Nevado Huascarán, Cordillera Blanca, Peru in 1962 and 1970, *Eng. Geol.,* **108**(1), 96–118.

Forterre, Y. & Pouliquen, O., 2003. Long-surface wave instability in dense granular flows, *J. Fluid. Mech.,* **486,** 21–50.

Gregoretti, C. & Fontana, G.D., 2008. The triggering of debris flow due to channel-bed failure in some alpine headwater basins of the Dolomites: analyses of critical runoff, *Hydrol. Process.,* **22,** 2248–2263.

Guzzetti, F., Peruccacci, S., Rossi, M. & Stark, C.P., 2008. The rainfall intensity — duration control of shallow landslides and debris flows: an update, *Landslides,* **5,** 3–11.

Haeberli, W., Huggel, C., Kaeaeb, A., Zgraggen-Oswald, S., Polkvoj, A., Galushkin, I., Zotikov, I. & Osokin, N., 2004. The Kolka-Karmadon rock/ice slide of 20 September 2002: an extraordinary event of historical dimensions in North Ossetia, Russian Caucasus, *J. Glaciol.,* **50**(171), 533–546.

Huebl, J., Gahnal, E., Gruber, H., Holub, M., Holzinger, G., Moser, M. & Pichler, A., 2004. Risikomanagement Lattenbach: Risikoanalyse. IAN Report 95 Band 1, Institute of Mountain Risk Engineering, University of Natural Resources and Life Sciences (unpublished report).

Huebl, J. & Kaitna, R., 2010. Sediment delivery from the Lattenbach catchment to the river Sanna by debris floods and debris flows, in *Proceedings of the International Symposium Interpraevent 2010,* Taiwan.

Ishihara, T., Iwagaki, Y. & Iwasa, Y., 1954. Theory of the roll-wave trains in laminar water flow on a steep slope surface—studies on the thin sheet flow, 5th report, *J. Jpn. Soc. Civil Eng.,* **19,** 46–57, in Japanese.

Iverson, R.M., 1997. The physics of debris flows, *Rev. Geophys.,* **35**(3), 245–296.

Iverson, R.M., Logan, M., LaHusen, R.G. & Berti, M., 2010. The perfect debris flow? Aggregated results from 28 large-scale experiments, *J. geophys. Res.,* **115,** doi:10.1029/2009JF001514.

Jeffreys, H.J., 1925. The flow of water in an inclined channel of rectangular section, *Phil. Mag., Ser. 6,* **49,** 793–807.

Johnson, C.G., Kokelaar, B.P., Iverson, R.M., Logan, M., LaHusen, R.G. & Gray, J.M.N.T., 2012. Grain-size segregation and levee formation in geophysical mass flows, *J. geophys. Res.,* **117,** F01032, doi:10.1029/2011JF002185.

Kaitna, R., Palucis, M.C., Yohannes, B., Hill, K.M. & Dietrich, W.E., 2011a. The effect of fines and grain size distribution on pore fluid pressure, shear rate and bulk flow resistance in large scale experimental debris flows, *Geophys. Res. Abstr.* 2011 (EP31C-0832).

Kaitna, R., Hsu, L., Rickenmann, D. & Dietrich, W.E., 2011b. On the development of an unsaturated front of debris flows, in *Proceedings of the 5th International Conference on Debris-Flow Hazards: Mitigation, Mechanics, Prediction and Assessment,* Padua, Italy, June 14–17, eds Genevois, R., Hamilton, D.L. & Prestininzi, A., pp. 351–358.

Liu, C.N., Dong, J.J., Peng, Y.F. & Huang, H.F., 2009. Effects of strong ground motion on the susceptibility of gully type debris flows, *Eng. Geol.,* **104,** 241–253.

Longo, S., 2011. Roll waves on a shallow layer of a dilatant fluid, *Eur. J. Mech. B/Fluids,* **30,** 57–67.

McCoy, S., Kean, J.W., Coe, J.A., Staley, D.M., Waskleswicz, T.A. & Tucker, G.E., 2010. Evolution of a natural debris flow: in situ measurements of flow dynamics, video imagery, and terrestrial laser scanning, *Geology,* **38,** 735–738, doi:10.1130/G30928.1.

Mikos, M., Cetina, M. & Brilly, M., 2004. Hydrologic conditions responsible for triggering the Stoze landslide, Slovenia, *Eng. Geol.,* **73**, 193–213.

Ng, C. & Mei, C.C., 1994. Roll waves on a shallow layer of mud modelled as a power-law fluid, *J. Fluid Mech.,* **263,** 151–183.

Phillips, R.J., Armstrong, R.C., Brown, R.A., Graham, A.L. & Abbot, J.R., 1992. A constitutive equation for concentrated suspensions that accounts for shear induced particle migration, *Phys. Fluids, A,* **4**(1), 30–40.

Prasad, S.N., Pal, D. & Roekens, M.J.M., 2000. Wave formation on a shallow layer of flowing grains, *J. Fluid Mech.,* **413,** 89–110.

Savage, S.B. & Hutter, K., 1989. The motion of a finite mass of granular material down a rough incline, *J. Fluid Mech.,* **199,** 177–215.

Schonfeld, B., 1996. Roll-waves in granular flows and debris flows, *M.S. thesis,* McGill Univ., Montreal, Que., Canada, 160 pp.

Suwa, H., 1988. Focusing mechanism of large boulders to a debris flow front, *Trans. Japan. Geomorph. Union,* **9,** 151–178.

Takahashi, T., 1980. Debris flow on prismatic open channel, *J. Hydr. Div., ASCE,* **106**(HY3), 381–396.

Takahashi, T., 1991. *Debris Flow: IAHR Monograph Series,* Balkema.

Takahashi, T., Nakagawa, H. & Ogata, M., 1998. Mechanics of the Viscous Type Debris Flow—Formation and Propagation of the Debris Flow Surge, Disaster Prevention Research Institute Annuals. B, Disaster Prevention Research Institute Kyoto University, **41,** B-2, 265–276, in Japanese.

Theule, J.I., Liebault, F., Loye, D., Laigle, D. & Jaboyedoff, M., 2012. Sediment budget monitoring of debris-flow and bedload transport in the Manival Torrent, SE France, *Nat. Haz. Earth Syst. Sci.,* **12,** 731–749.

Zanuttigh, B. & Lamberti, A., 2002. Roll waves simulation using shallow water equations and weighted average flux method, *J. Hydr. Res.,* **40**(5), 610–622.

Zanuttigh, B. & Lamberti, A., 2004. Analysis of debris wave development using 1D shallow water equations, *J. Hydr. Eng.,* **1304,** 293–304.

Zanuttigh, B. & Lamberti, A., 2007. Instability and surge development in debris flows, *Rev. Geophys.,* **45,** RG3006, doi:10.1029/2005RG000175.

APPENDIX A:

Derivation of eq. (32), (33) and (34):

First, eq. (30) is transformed as follows,

$$\frac{v}{U_*} = \frac{1}{\kappa}\left[\sinh^{-1}\left\{\frac{1}{\phi_0}\left(\frac{h}{d}\right)\right\} - \sinh^{-1}\left\{\frac{1}{\phi_0}\left(\frac{y_0}{d}\right)\right\} - \sqrt{1+{\phi_0}^2\left(\frac{d}{h}\right)^2}\,\phi_0\left(\frac{d}{h}\right) + \phi_0\left(\frac{d}{h}\right)\right]; \tag{A1}$$

here,

$${\phi_0}^2 = \lambda^2\left(\frac{a_i \sin\alpha}{\kappa^2}\right)\left(\frac{\sigma}{\rho_m}\right), \quad \phi^2 = {\phi_0}^2\left(\frac{d}{h}\right)^2. \tag{A2}$$

The momentum correction factor β is defined as

$$\beta = \frac{1}{h}\int_0^h \left(\frac{u}{v}\right)^2 \mathrm{d}y = \frac{1}{h}\int_0^1 \left(\frac{u}{v}\right)^2 \mathrm{d}Y \cdot h = \int_0^1 \left(\frac{u}{v}\right)^2 \mathrm{d}Y. \tag{A3}$$

Therefore, u in eq. (29) and v in eq. (A1) are substituted in eq. (A3), and β is obtained as

$$\beta_{tc} = \left[\left\{\sinh^{-1}\left(\frac{1}{\phi}\right)\right\}^2 - 2\left\{\sqrt{1+\phi^2} + \sinh^{-1}\left(\frac{Y_0}{\phi}\right)\right\}\cdot\sinh^{-1}\left(\frac{1}{\phi}\right) + 2\left\{\sqrt{1+\phi^2} - \phi\right\}\cdot\sinh^{-1}\left(\frac{Y_0}{\phi}\right) + \left\{\sinh^{-1}\left(\frac{Y_0}{\phi}\right)\right\}^2 + 2\right]$$
$$\times\left[\sinh^{-1}\left(\frac{1}{\phi}\right) - \sinh^{-1}\left(\frac{Y_0}{\phi}\right) - \sqrt{1+\phi^2} + \phi\right]^{-2}. \tag{A4}$$

The friction factor f' is defined by the relation $v/U_* = \sqrt{2/f'}$, from which with the aid of eq. (A1)

$$f' = 2\kappa^2\left[\sinh^{-1}\left\{\frac{1}{\phi_0}\left(\frac{H}{d}\right)\right\} - \sinh^{-1}\left\{\frac{1}{\phi_0}\left(\frac{y_0}{d}\right)\right\} - \sqrt{1+{\phi_0}^2\left(\frac{d}{H}\right)^2} + \phi_0\left(\frac{d}{H}\right)\right]^{-2}$$

is obtained. From this, $(H/f')(\mathrm{d}f'/\mathrm{d}H)$ can be deduced as

$$\frac{H}{f'}\left(\frac{\mathrm{d}f'}{\mathrm{d}H}\right) = -2\left[\sinh^{-1}\left\{\frac{1}{\phi_0}\left(\frac{H}{d}\right)\right\} - \sinh^{-1}\left\{\frac{1}{\phi_0}\left(\frac{y_0}{d}\right)\right\} - \sqrt{1+{\phi_0}^2\left(\frac{d}{H}\right)^2} + \phi_0\left(\frac{d}{H}\right)\right]^{-1}$$
$$\times\left[\frac{\frac{1}{\phi_0}\left(\frac{H}{d}\right)}{\sqrt{1+\frac{1}{{\phi_0}^2}\left(\frac{H}{d}\right)^2}} + \frac{{\phi_0}^2\left(\frac{d}{H}\right)^2}{\sqrt{1+{\phi_0}^2\left(\frac{d}{H}\right)^2}} - \phi_0\left(\frac{d}{H}\right)\right]. \tag{A5}$$

For a rectangular channel and a flow with $B \ll H$, the simplified relations $R \approx H$, $m = 1$ and $\partial A/\partial H = B$ are used; eq. (A5) is then substituted into eq. (23) or (24), implying

$$\left[\frac{\frac{1}{\phi_0}\left(\frac{H}{d}\right)}{\sqrt{1+\frac{1}{{\phi_0}^2}\left(\frac{H}{d}\right)^2}}+\frac{{\phi_0}^2\left(\frac{d}{H}\right)^2}{\sqrt{1+{\phi_0}^2\left(\frac{d}{H}\right)^2}}-\phi_0\left(\frac{d}{H}\right)\right]\times\left[\sinh^{-1}\left\{\frac{1}{\phi_0}\left(\frac{H}{d}\right)\right\}-\sinh^{-1}\left\{\frac{1}{\phi_0}\left(\frac{y_0}{d}\right)\right\}-\sqrt{1+{\phi_0}^2\left(\frac{d}{H}\right)^2}+\phi_0\left(\frac{d}{H}\right)\right]^{-1}$$
$$\geq\left(\beta-\frac{3}{2}\right)+\sqrt{\beta(\beta-1)+\frac{1}{{F_r}^2}}. \tag{A6}$$

This can also be expressed as

$$F_r \geq \frac{1}{\sqrt{\left\{\Phi_{tc}+\left(\frac{3}{2}-\beta_{tc}\right)\right\}^2-\beta_{tc}\,(\beta_{tc}-1)}}, \tag{A7}$$

with

$$\Phi_{tc}=\left[\sqrt{1+{\phi_0}^2\left(\frac{d}{H}\right)^2}-\phi_0\left(\frac{d}{H}\right)\right]\left[\sinh^{-1}\left\{\frac{1}{\phi_0}\left(\frac{H}{d}\right)\right\}-\sinh^{-1}\left\{\frac{1}{\phi_0}\left(\frac{y_0}{d}\right)\right\}-\sqrt{1+{\phi_0}^2\left(\frac{d}{H}\right)^2}+\phi_0\left(\frac{d}{H}\right)\right]^{-1}. \tag{A8}$$

APPENDIX B:

Derivation of eqs (40), (41) and (42):
The velocity profile of a laminar flow model with yield criterion is defined by eq. (37),

$$\frac{u}{U_*}=\frac{1}{2}\,\varphi_c\,R_*\left[\left(1-\frac{{U_{*_\eta}}^2}{{U_*}^2}\right)^2-\left\{\left(1-\frac{{U_{*_\eta}}^2}{{U_*}^2}\right)-\left(\frac{y}{h}\right)\right\}^2\right]$$

where $\varphi_c=(1-C/C_*)^{1.82}\,(1+\epsilon\,C)$, $R_*=U_*h/\nu$, $\nu=\mu/\rho_m$, $\rho_m=\{\rho+(\sigma-\rho)C\}$, $\epsilon=\sigma/\rho-1$, ${U_{*_\eta}}^2=\tau_\eta/\rho_m$, ${U_*}^2=g\,h\sin\theta$. τ_η is the yield stress at $y=y_\eta$.
Generally, the mean velocity v is defined as

$$v=\frac{1}{h}\int_0^h u\mathrm{d}y=\frac{1}{h}\left\{\int_0^{y_\eta}u\,\mathrm{d}y+\int_{y_\eta}^h u\,\mathrm{d}y\right\}, \tag{B1}$$

so we derive the mean velocity of this model as

$$\frac{v}{U_*}=\frac{1}{2}\,\varphi_c\,R_*\left\{\frac{2}{3}{a_\eta}^2-\left(2-\frac{{U_{*_\eta}}^2}{{U_*}^2}\right)a_\eta+2\left(1-\frac{{U_{*_\eta}}^2}{{U_*}^2}\right)\right\}a_\eta \tag{B2}$$

with $a_\eta=y_\eta/h$.

Moreover, when the sheared flow layer is defined by $y=y_\eta$, $a_\eta=y_\eta/h$ is the ratio of shear height to flow height (so, the plug height is $y-y_\eta$). Consequently, if $a_\eta=1$ the flow is sheared over the whole depth and $a_\eta=0$. In this case the flow is only sheared very close to the bottom. We also conclude that $\left(1-{U_{*_\eta}}^2/{U_*}^2\right)$ equals a_η. Using a_η, eq. (B2) is expressed as,

$$\frac{v}{U_*}=\frac{1}{6}\,\varphi_c\,R_*\,(3-a_\eta)\,{a_\eta}^2. \tag{B3}$$

The momentum correction factor β is defined by eq. (A3); thus, substituting u of eq. (37) and v from (B2) into (A3) we derive β as,

$$\beta=\frac{3\left\{60{\varphi_B}^2-2a_\eta\,\varphi_B\,(3+2\varphi_B)+{a_\eta}^2\,(3+45\,\varphi_B)\right\}}{5\left\{2\,{a_\eta}^2+6\,\varphi_B-3\,a_\eta\,(1+\varphi_B)\right\}^2}, \tag{B4}$$

where, $\varphi_B=\left(1-{U_{*_\eta}}^2/{U_*}^2\right)$. When using $\varphi_B=a_\eta$, it is possible to express the above equation as,

$$\beta=\frac{3\,(15-7a_\eta)}{5\,(a_\eta-3)^2}. \tag{B5}$$

As a_η varies from $a_\eta=0$ at the bottom to $a_\eta=1$ at the surface, β has values $\beta=1$ to $6/5$ depending on the depth of the unsheared layer. The mean velocity of eq. (B3) can be expressed, using the variable H, as

$$\frac{v}{U_*}=\frac{1}{6}\,\varphi_c\,\frac{\sqrt{g\,\sin\theta}}{\nu}\,(3-a_\eta)\,a_\eta\,H^{\frac{3}{2}}. \tag{B6}$$

From $v/U_* = \sqrt{2/f'}$ and eq. (B6), we deduce

$$\frac{H}{f'}\left(\frac{df'}{dH}\right) = -3.$$

Thus, for a rectangular channel and with $B \ll H$ and $R \approx H$, $m = 1$ and $\partial A/\partial H = B$, we derive the instability condition from eq. (26) and obtain

$$F_r \geq \frac{1}{\sqrt{(3-\beta)^2 - \beta\,(\beta-1)}} = \frac{1}{\sqrt{9-5\,\beta}} \tag{B7}$$

with $\beta = (3/5)(15 - 7a_\eta)/(a_\eta - 3)^2$.

Using a_η instead of β, relation (B7) assumes the form

$$F_r \geq \frac{1}{\sqrt{\dfrac{36 - 33\,a_\eta + 9\,a_\eta{}^2}{\left(a_\eta - 3\right)^2}}}. \tag{B8}$$

We can conclude that criticality occurs when $F_r \geq 1/2$ for $a_\eta = 0$ and $F_r \geq 1/\sqrt{3} \simeq 0.573$ for $a_\eta = 1$. Therefore, threshold values of F_r separating stable and instable conditions vary from $1/2 = 0.5$ to $1/\sqrt{3} \simeq 0.573$.

APPENDIX C:

Derivation of eq. (47):

Rewriting eq. (45) with $h = H$, we obtain

$$\frac{v}{U_*} = \frac{2}{5}\left[\frac{1}{a_i \sin\alpha}\left\{C + (1-C)\,\frac{\rho}{\sigma}\right\}\right]^{\frac{1}{2}}\left\{\left(\frac{C_*}{C} - 1\right)^{\frac{1}{3}} - 1\right\}\left(\frac{H}{d}\right). \tag{C1}$$

The momentum correction factor β is defined by eq. (A3); thus, substituting u from (44) and v from (45) into (A3) yields β

$$\beta = \frac{5}{4},$$

corroborating (46). From $v/U_* = \sqrt{2/f'}$ and eq. (C1), we obtain

$$\frac{H}{f'}\left(\frac{\mathrm{d}f'}{\mathrm{d}H}\right) = -2.$$

Therefore, for a rectangular channel and $B \ll H$, we have, as before $R \approx H$, $m = 1$ and $\partial A/\partial H = B$ and may derive the instability condition from (26),

$$F_r \geq \frac{2}{\sqrt{5}} \simeq 0.894,$$

which confirms (47).